ChemComm

COMMUNICATION

View Article Online
View Journal | View Issue

Cite this: *Chem. Commun.*, 2021, **57**, 5634

Received 23rd March 2021,
Accepted 29th April 2021

DOI: 10.1039/d1cc01570b

rsc.li/chemcomm

Pure organic quinacridone dyes as dual sensitizers in tandem photoelectrochemical cells for unassisted total water splitting†

Luze Shen,‡[a] Shicong Zhang,‡[a] Haoran Ding,[a] Fushuang Niu,[b] Yanmeng Chu,[c] Wenjun Wu, *[a] Yue Hu, [c] Ke Hu *[b] and Jianli Hua *[a]

Pure organic dye QAP-C8 based on quinacridone (QA) with octyl side chains as the donor and pyridine dicarboxylic acid (PDA) as the acceptor was first used in both the photoanode and the photocathode of photoelectrochemical cells. A tandem device with QAP-C8 as the photosensitizer realized overall water splitting and showed a STH of 0.11% under neutral pH conditions without an external bias.

Dye-sensitized photoelectrochemical cells (DSPECs) continue to be one of the most ideal candidates to realize the conversion of light to hydrogen energy.[1,2] DSPECs use molecular dyes that can be easily tuned to absorb the visible part of the solar spectrum. Nowadays, most of the dyes used in DSPECs are ruthenium-based polypyridyl complexes, but the low natural abundance of the ruthenium metal and the long term instability of its oxidized forms impede their development.[3] Pure organic dyes are very promising alternatives due to their low cost, adjustable molecular orbitals, and structural diversity.[4] Various pure organic dyes have been investigated for DSPECs so far, including perylene imide,[5–9] triarylamine,[10–14] diketopyrrolopyrrole (DPP),[15] organic polymer chromophores[16,17] and other small molecule organic chromophores.[18–22] However, most of the dyes show a narrow absorption spectrum ($\lambda_{max} < 400$ nm) and poor stability. So, the design of dye molecules with a broad optical response, appropriate energy levels, and good stability for DSPECs is urgently needed.

In this work, we designed three A–D–A type dyes (**QAP-C4**, **QAP-C8**, and **QAP-C16**) based on quinacridone (QA) with butyl, octyl and hexadecyl side chains as the electron donor, and PDA as the anchoring group (Scheme 1). In terms of the stability of dyes, QA derivatives have good planarity, and excellent photoelectrochemical properties and photothermal stability.[23,24] The aliphatic side chains are expected to prevent the dyes from flopping down to the hydrophilic titania surface while the dual carboxylic acid groups provide one covalent linkage with the titanol group and the other with molecular catalysts through Zr^{4+} ions.[25–29] PDA is insoluble in aqueous solutions and does not desorb from semiconductors, which is favorable for the stability of DSPECs.[30] In terms of the absorption spectra of dyes, the introduction of PDA makes the absorption of dyes exhibit a red-shift and broadens the absorption spectrum. Therefore, these dyes are expected to be used in high efficiency DSPECs.

For the photoanode, it is difficult for pure organic dyes to meet the energy level of water oxidation.[31] The results of photophysical, electrochemical and DFT calculations showed that the holes of dyes can be injected from the highest occupied molecular orbital (HOMO) of the dye into the water oxidation catalyst (WOC) **RuOEC** thermodynamically. After self-assembly with Zr^{4+} ions and **RuOEC**, **QAP-C8** and **QAP-C16** were able to construct a layer-by-layer photoanode, and then drive the water oxidation reaction. The photocathode was prepared by co-adsorbing

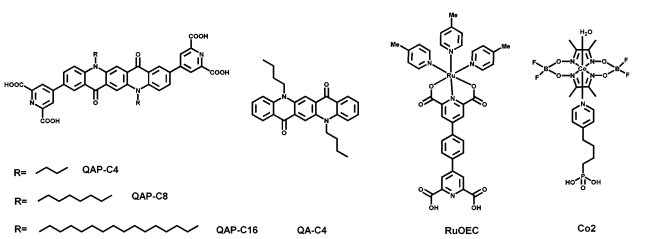

Scheme 1 The structures of **QAP-C4**, **QAP-C8**, **QAP-C16**, **QA-C4**, **RuOEC** and **Co2**.

[a] *Key Laboratory for Advanced Materials, Institute of Fine Chemicals, School of Chemistry and Molecular Engineering, East China University of Science and Technology, 130 Meilong Road, Shanghai, 200237, P. R. China. E-mail: jlhua@ecust.edu.cn, wjwu@ecust.edu.cn*

[b] *Department of Chemistry, Fudan University, 220 Handan Road, Shanghai 200433, P. R. China. E-mail: khu@fudan.edu.cn*

[c] *Michael Grätzel Center for Mesoscopic Solar Cells, Wuhan National Laboratory for Optoelectronics, Huazhong University of Science and Technology, 1056 Luoyu Road, Wuhan 430074, Hubei, P. R. China*

† Electronic supplementary information (ESI) available: Experimental details, characterization data, and additional spectra. See DOI: 10.1039/d1cc01570b

‡ L. S. and S. Z. equally contributed to this work as the first authors.

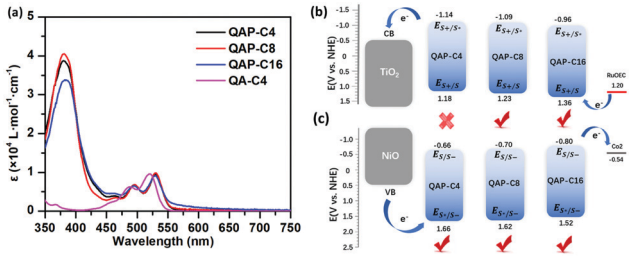

Fig. 1 (a) The molar extinction coefficient spectra of dyes in DMSO solution. (b and c) Energetics of the ground and excited state redox potentials of **QAP-C4**, **QAP-C8** and **QAP-C16** at the photoanode (b) and at the photocathode (c).

QAP dyes and hydrogen evolution catalyst (HEC) **Co2** on mesoporous NiO. In the end, **QAP-C8** was found to be useful both in the photoanode and photocathode in a bias-free tandem device due to its suitable energy band, which is the first tandem device based on the same organic dye. Encouragingly, an overall water splitting photocurrent of 114.1 μA cm^{-2} was obtained (under no bias, pH = 7). The solar to hydrogen (STH) conversion efficiency of tandem DSPECs was calculated to be 0.11%, which is the highest value for tandem DSPECs as far as we know.[11,22,32] These results provide a new strategy for the design of photosensitizers with a visible light spectrum and stability in the construction of artificial photosynthesis devices.

The molar extinction coefficient spectra of dyes (**QA-C4**, **QAP-C4**, **QAP-C8** and **QAP-C16**) in dilute solutions of DMSO are shown in Fig. 1a. **QA-C4** without PDA showed two absorption peaks at 488 nm and 522 nm. **QAP-C4**, **QAP-C8** and **QAP-C16** showed one extra strong absorption band peaked at ~380 nm while the other two visible bands slightly red shifted compared with **QA-C4**. The characteristic absorption peaks between 360 and 400 nm were attributed to intramolecular charge transfer (ICT) according to the DFT calculation results. The electron densities of the HOMO and LUMO were primarily delocalized at the **QAP** donor moiety, while the LUMO+1 could extend to the acceptor PDA part (Table S1, ESI†). Furthermore, this absorption band at ~380 nm mainly originated from the HOMO to the LUMO+1 (Table S2, ESI†). Therefore, the transition could be attributed to an ICT process.

Cyclic voltammetry (CV) was used to determine the ground state redox potentials of **QAP-C4**, **QAP-C8**, and **QAP-C16** (Fig. S3a, ESI†). The excited state redox potentials were calculated from the electrochemical data and the intersection of the normalized absorption and emission (Fig. S4, ESI†). The results are summarized in Table S3 (ESI†). Several key factors were considered for a working tandem DSPEC device. For the photoanode (Fig. 1b): (i) the excited state reduction potentials (E_{S+/S^*}) of dyes are more negative than the conduction band (CB) of TiO_2 (−0.5 V), ensuring that the electrons of the excited dye can be successfully injected into the CB of TiO_2 from their lowest unoccupied molecular orbital (LUMO). (ii) The onset potential of **RuOEC** is 1.2 V *vs.* NHE (pH = 7).[11] Hence, the oxidized states of **QAP-C8** and **QAP-C16** can donate holes to **RuOEC** from their HOMO. With the increase of the alkyl length of side chains, the ground state oxidation potentials ($E_{S+/S}$) of the three dyes become more positive, while the ($E_{S+/S}$) values were almost the same after the co-adsorption of the dye and **CDCA** (Fig. S3b, ESI†).[10] Therefore, we speculate that the more positive $E_{S+/S}$ of **QAP-C16** may be due to the aggregation of dye molecules. For the photocathode (Fig. 1c): (i) the excited state oxidation potentials ($E_{S^*/S-}$) of the three dyes are more positive than the valence band (VB) of NiO, ensuring that the holes of the excited dye can be successfully injected into the VB of NiO from their LUMO. (ii) The ground state reduction potentials ($E_{S/S-}$) of the three dyes are more negative than the onset potential of **Co2**. Therefore, the reductively quenched excited state can reduce **Co2** from their LUMOs. In addition, the electron or hole transfer between the dye and catalyst was proved to be the rate-limiting step in DSPECs.

Long-life reduced or oxidized dyes are beneficial to the stability of a device. Absorption spectra of the reduced (Fig. S5a, ESI†) and oxidized dyes (Fig. S5b, ESI†) were detected by spectroelectro-chemical measurements. For the photoanode, the absorption of the dye changed as the applied bias became more positive and reached a steady state when the applied bias reached $E_{S+/S}$. This proved that the dye had donated electrons to form the oxidized state through the applied bias. For the photocathode, as the applied bias became more negative, the absorption of the dye changed and reached a steady state when the applied bias reached $E_{S/S-}$. This proved that the dye had obtained electrons to form the reduced state through the applied bias.[28,33] The result of spectroelectro-chemical measurements proved that long-life reduced or oxidized dyes were obtained through the applied bias.

QAP dyes and **RuOEC** were self-assembled layer by layer through the Zr^{4+} ion linker on the TiO_2 film to form TiO_2|**QAP-C8**|Zr^{4+}|**RuOEC** and TiO_2|**QAP-C16**|Zr^{4+}|**RuOEC** electrodes as photoanodes (Fig. S6a, ESI†), and the photoelectrochemical properties of the photoanodes were measured.

Linear scanning voltammetry (LSV) curves are shown in Fig. S6bc (ESI†). The photocurrent of the TiO_2|**QAP-C8**|Zr^{4+}|**RuOEC** electrode started to generate a positive current at −0.54 V *vs.* NHE (pH = 7) and reached a plateau at −0.40 V *vs.* NHE (pH = 7) under illumination, where the photocurrent density was about 184 μA cm^{-2}. The photocurrent of the TiO_2|**QAP-C16**|Zr^{4+}|**RuOEC** electrode started to generate a positive current at −0.56 V and reached a plateau at −0.40 V under illumination, where the photocurrent density was about 223 μA cm^{-2}. These values were higher than the current density in the dark, indicating the photoactivity of the prepared photoanode.

Here we choose 0.2 V and 0.3 V *vs.* NHE (pH = 7) as the applied bias to measure the transient current responses to on–off cycles of two electrodes, respectively (Fig. 2a and b). They produced a photocurrent density of 213 μA cm^{-2} and 253 μA cm^{-2} after light illumination of 100 s. Monochromatic incident photon-to-current efficiency (IPCE) measurements were performed (Fig. S7, ESI†). For TiO_2|**QAP-C8**|Zr^{4+}|**RuOEC** and TiO_2|**QAP-C16**|Zr^{4+}|**RuOEC**, the IPCE at 520 nm was 2.5% and 6.0%, respectively. The shape of the IPCE curves is similar to the UV-vis spectra, showing that dyes can effectively absorb the visible light and achieve photon-to-current conversion. The

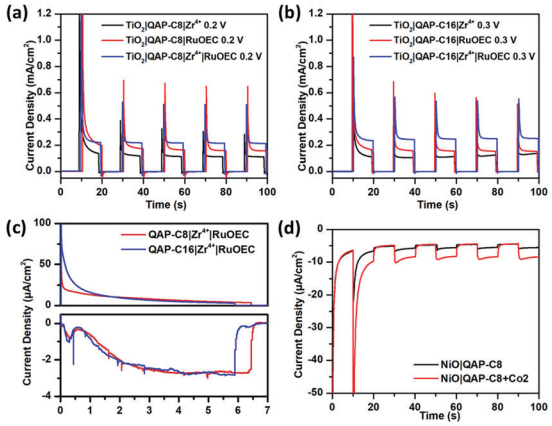

Fig. 2 (a and b) Transient current responses to on–off cycles for **QAP-C8** and **QAP-C16** at an applied bias potential of 0.2 V and 0.3 V *vs.* NHE (pH = 7). (c) Current density–time curve of the generator/collector photoanodes. (d) Transient current responses to on–off cycles for **QAP-C8** at an applied bias potential of −0.1 V *vs.* NHE (pH = 7).

photocurrent density of TiO_2|**QAP-C8**|Zr^{4+}|**RuOEC** and TiO_2|**QAP-C16**|Zr^{4+}|**RuOEC** electrodes in 6 hours of the long-time test was measured (Fig. 2c) and the corresponding amount of oxygen generated was measured by the collector–generator method. With oxygen generated at the photoanode diffusing through the collector–generator gap, the amount of oxygen detected by the collector electrode slowly increased. The current density of the collector electrodes finally plateaued at 2.7 μA cm^{-2} and 2.8 μA cm^{-2}. The faradaic efficiencies (η_{oxygen}) of **QAP-C8** and **QAP-C16** were calculated to be 33% and 27% according to eqn (1) in the ESI.† These results clearly demonstrated that light-driven water oxidation was successfully achieved by assembling the catalyst **RuOEC** and organic photosensitizer on TiO_2.

For the photocathode, all three **QAP** dyes had the potential for hydrogen production according to Fig. 1c. We prepared NiO|**QAP-C4** + **Co2**, NiO|**QAP-C8** + **Co2** and NiO|**QAP-C16** + **Co2** photocathodes through the co-adsorbed dyes and **Co2** on the NiO film (Fig. S9a, ESI†). The LSV and *i*–*t* measurements showed that the three photocathodes gave similar performance (Fig. 2d and Fig. S9b–f, ESI†). The NiO|**QAP-C8** + **Co2** electrode showed the highest photocurrent density. The photocurrent increased rapidly at bias voltages from 0.5 V to 0.3 V *vs.* NHE (pH = 7) and reached plateaus at $E < -0.1$ V *vs.* NHE (pH = 7) with about −30 μA·cm^{-2}.

The results of photoelectrochemical measurements showed that dyes based on quinacridone as the donor and PDA as the anchor group can be used both on the photoanode and the photocathode. After the photoanode and the photocathode are irradiated, photogenerated charges can be cycled through the tandem DSPECs (Fig. 3a). After the photoanode dyes were excited by light, the electrons and holes were injected into TiO_2 and **RuOEC** to realize water oxidation, respectively. For the photocathode, holes and electrons were injected into NiO and **Co2**, respectively. Finally, the two electrodes circulated the charge through a copper wire. The performances of the tandem

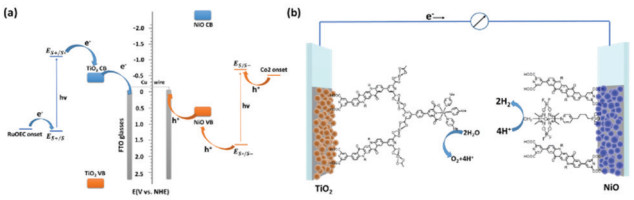

Fig. 3 (a) Schematic energy diagram for **QAP-C8**, **RuOEC**, **Co2**, FTO, TiO_2, and NiO and the electron transfer direction (pH = 7). (b) The diagram of a two-electrode tandem DSPEC, with TiO_2|**QAP-C8**|Zr^{4+}|**RuOEC** as the photoanode.

DSPECs were usually limited by the photocathode. Hence, we selected **QAP-C8** as the photosensitizer to construct a two-electrode tandem PEC cell because **QAP-C8** showed the best performance in the photocathode. In addition, the starting potentials of TiO_2|**QAP-C8**|Zr^{4+}|**RuOEC** and NiO|**QAP-C8** + **Co2** were around −0.2 and 0 V *vs.* NHE (pH = 7), respectively. The starting potentials of the photoanode were more negative. Hence, a bias-free two-electrode tandem DSPEC was constructed for overall water-splitting (Fig. 3b).

We designed three configurations depending on the direction of illumination (Fig. 4a). In configuration 1, the photoanode and photocathode were both illuminated. In configurations 2 and 3, only the photoanode and photocathode were illuminated, respectively. In configuration 1, LSV showed that the photocurrent reached a plateau from −0.1 V to 0.5 V *vs.* NHE (pH = 7), indicating that it could work without an applied bias and the photocurrent was 96 μA cm^{-2} (Fig. 4b). Then, we measured the transient current responses to light cycles without an applied bias (Fig. 4c). In configuration 1, the highest current density of 114.1 μA cm^{-2} was obtained, and it was still maintained at 69.3 μA cm^{-2} after 15 min (Fig. S10, ESI†). The plots of evolved H_2/O_2 yield against irradiation time are shown in Fig. S11 (ESI†). After 15 min, 0.43 μmol of H_2 was produced, corresponding to a faradaic efficiency ($\eta_{hydrogen}$) of 89%. Configuration 3 showed higher photocurrent density (58.6 μA cm^{-2}) than configuration 2 (43.1 μA cm^{-2}), because the smaller current density of the

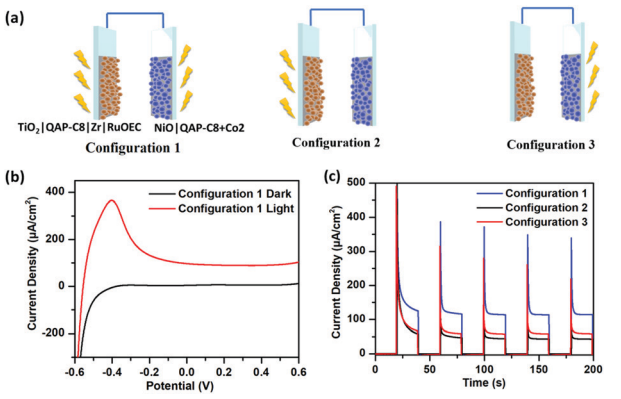

Fig. 4 (a) Configurations of three different lighting methods. (b) LSV of a two-electrode tandem DSPEC. (c) Transient current responses to on–off cycles of a two-electrode tandem DSPEC with different directions of light illumination.

photocathode limited the performance of tandem DSPECs. When light was irradiated from the photoanode, most of the light was utilized by the photoanode. The optical power density at the photocathode was relatively lower, leading to the decrease of photocurrent. With the optimal lighting method, the STH was calculated to be 0.11%, according to eqn (2) and (4) shown in the ESI.†

In summary, three A–D–A organic compounds (**QAP-C4**, **QAP-C8** and **QAP-C16**) based on quinacridone with butyl, octyl and hexadecyl side chains as the donor and PDA as the acceptor have been successfully used as photosensitizers in both photoanodes and photocathodes. Optical and electrochemical experiments showed that the side chains of **QAP-C4**, **QAP-C8** and **QAP-C16** had little effect on the absorption spectra and band gap of the dyes, but their HOMO levels gradually became more positive (1.18 V, 1.23 V and 1.36 V *vs.* NHE (pH = 7), respectively). Therefore, **QAP-C8** and **QAP-C16** were successfully used to construct *n*-DSPEC. For the *p*-DSPEC, **QAP-C8** showed the best performance. On this basis, we successfully constructed a tandem DSPEC device, based on the same organic dye **QAP-C8** as the photosensitizer incorporated in both the photoanode and the photocathode for the first time. When light was irradiated from both sides, a STH of 0.11% was realized with no bias. These results provided new guidance for the design of molecular DSPECs and broad prospects for the future construction of artificial photosynthesis devices.

For financial support of this research, we thank the project supported by the National Natural Science Foundation of China (21971064, 21872037 and 21772040), the Shanghai Science and Technology Committee (17520750100), the Shanghai Municipal Science and Technology Major Project (Grant No. 2018 SHZDZX03), the Fundamental Research Funds for the Central Universities (222201717003 and 50321101918001) and the Programme of Introducing Talents of Discipline to Universities (B16017). The authors thank the Research Center of Analysis and Test of East China University of Science and Technology for the help with characterization.

Conflicts of interest

There are no conflicts to declare.

Notes and references

1 Y. Zhu, D. Wang, Q. Huang, J. Du, L. Sun, F. Li and T. J. Meyer, *Nat. Commun.*, 2020, 11.
2 S. Zhang, H. Ye, J. Hua and H. Tian, *EnergyChem*, 2019, **1**, 100015.
3 J. T. Hyde, K. Hanson, A. K. Vannucci, A. M. Lapides, L. Alibabaei, M. R. Norris, T. J. Meyer and D. P. Harrison, *ACS Appl. Mater. Interfaces*, 2015, **7**, 9554–9562.
4 P. Xu, N. S. McCool and T. E. Mallouk, *Nano Today*, 2017, **14**, 42–58.
5 K. A. Click, D. R. Beauchamp, Z. Huang, W. Chen and Y. Wu, *J. Am. Chem. Soc.*, 2016, **138**, 1174–1179.
6 F. Ronconi, Z. Syrgiannis, A. Bonasera, M. Prato, R. Argazzi, S. Caramori, V. Cristino and C. A. Bignozzi, *J. Am. Chem. Soc.*, 2015, **137**, 4630–4633.
7 M. T. Vagnini, A. L. Smeigh, J. D. Blakemore, S. W. Eaton, N. D. Schley, F. D'Souza, R. H. Crabtree, G. W. Brudvig, D. T. Co and M. R. Wasielewski, *Proc. Natl. Acad. Sci. U. S. A.*, 2012, **109**, 15651–15656.
8 B. Xu, L. Tian, A. S. Etman, J. Sun and H. Tian, *Nano Energy*, 2019, **55**, 59–64.
9 K. Yun, S. Zhang, F. Yu, H. Ye and J. Hua, *J. Energy Chem.*, 2018, **27**, 728–735.
10 N. Kaeffer, J. Massin, C. Lebrun, O. Renault, M. Chavarot-Kerlidou and V. Artero, *J. Am. Chem. Soc.*, 2016, **138**, 12308–12311.
11 F. Li, K. Fan, B. Xu, E. Gabrielsson, Q. Daniel, L. Li and L. Sun, *J. Am. Chem. Soc.*, 2015, **137**, 9153–9159.
12 L. Li, L. Duan, F. Wen, C. Li, M. Wang, A. Hagfeldt and L. Sun, *Chem. Commun.*, 2012, **48**, 988–990.
13 J. Massin, M. Bräutigam, S. Bold, M. Wächtler, M. Pavone, A. B. Muñoz-García, B. Dietzek, V. Artero and M. Chavarot-Kerlidou, *J. Phys. Chem. C*, 2019, **123**, 17176–17184.
14 M. S. Eberhart, D. Wang, R. N. Sampaio, S. L. Marquard, B. Shan, M. K. Brennaman, G. J. Meyer, C. Dares and T. J. Meyer, *J. Am. Chem. Soc.*, 2017, **139**, 16248–16255.
15 Y. Farré, L. Zhang, Y. Pellegrin, A. Planchat, E. Blart, M. Boujtita, L. Hammarström, D. Jacquemin and F. Odobel, *J. Phys. Chem. C*, 2016, **120**, 7923–7940.
16 A. Krawicz, J. Yang, E. Anzenberg, J. Yano, I. D. Sharp and G. F. Moore, *J. Am. Chem. Soc.*, 2013, **135**, 11861–11868.
17 D. M. Ryan, M. K. Coggins, J. J. Concepcion, D. L. Ashford, Z. Fang, L. Alibabaei, D. Ma, T. J. Meyer and M. L. Waters, *Inorg. Chem.*, 2014, **53**, 8120–8128.
18 D. Badgurjar, B. Shan, A. Nayak, L. Wu, R. Chitta and T. J. Meyer, *ACS Appl. Mater. Interfaces*, 2020, **12**, 7768–7776.
19 Y. K. Eom, L. Nhon, G. Leem, B. D. Sherman, D. Wang, L. Troian-Gautier, S. Kim, J. Kim, T. J. Meyer, J. R. Reynolds and K. S. Schanze, *ACS Energy Lett.*, 2018, **3**, 2114–2119.
20 J. M. Gardner, M. Beyler, M. Karnahl, S. Tschierlei, S. Ott and L. Hammarstrom, *J. Am. Chem. Soc.*, 2012, **134**, 19322–19325.
21 T. M. McCormick, Z. Han, D. J. Weinberg, W. W. Brennessel, P. L. Holland and R. Eisenberg, *Inorg. Chem.*, 2011, **50**, 10660–10666.
22 C. D. Windle, H. Kumagai, M. Higashi, R. Brisse, S. Bold, B. Jousselme, M. Chavarot-Kerlidou, K. Maeda, R. Abe, O. Ishitani and V. Artero, *J. Am. Chem. Soc.*, 2019, **141**, 9593–9602.
23 H.-J. Song, D.-H. Kim, E.-J. Lee, S.-W. Heo, J.-Y. Lee and D.-K. Moon, *Macromolecules*, 2012, **45**, 7815–7822.
24 C. Wang, Z. Zhang and Y. Wang, *J. Mater. Chem. C*, 2016, **4**, 9918–9936.
25 B. Shan, A. Nayak, M. K. Brennaman, M. Liu, S. L. Marquard, M. S. Eberhart and T. J. Meyer, *J. Am. Chem. Soc.*, 2018, **140**, 6493–6500.
26 D. Wang, Y. Wang, M. D. Brady, M. V. Sheridan, B. D. Sherman, B. H. Farnum, Y. Liu, S. L. Marquard, G. J. Meyer, C. J. Dares and T. J. Meyer, *Chem. Sci.*, 2019, **10**, 4436–4444.
27 M. V. Sheridan, B. D. Sherman, R. L. Coppo, D. Wang, S. L. Marquard, K.-R. Wee, N. Y. Murakami Iha and T. J. Meyer, *ACS Energy Lett.*, 2016, **1**, 231–236.
28 D. Wang, R. N. Sampaio, L. Troian-Gautier, S. L. Marquard, B. H. Farnum, B. D. Sherman, M. V. Sheridan, C. J. Dares, G. J. Meyer and T. J. Meyer, *J. Am. Chem. Soc.*, 2019, **141**, 7926–7933.
29 X. Ding, Y. Gao, L. Zhang, Z. Yu, J. Liu and L. Sun, *ACS Catal.*, 2014, **4**, 2347–2350.
30 K. Fan, F. Li, L. Wang, Q. Daniel, E. Gabrielsson and L. Sun, *Phys. Chem. Chem. Phys.*, 2014, **16**, 25234–25240.
31 D. Wang, L. Wang, M. D. Brady, C. J. Dares, G. J. Meyer, T. J. Meyer and J. J. Concepcion, *J. Phys. Chem. C*, 2019, **123**, 30039–30045.
32 B. D. Sherman, M. V. Sheridan, K. R. Wee, S. L. Marquard, D. Wang, L. Alibabaei, D. L. Ashford and T. J. Meyer, *J. Am. Chem. Soc.*, 2016, **138**, 16745–16753.
33 B. N. DiMarco, T. C. Motley, R. S. Balok, G. Li, M. A. Siegler, R. M. O'Donnell, K. Hu and G. J. Meyer, *J. Phys. Chem. C*, 2016, **120**, 14226–14235.